AMERICAN SOCIETY FOR MICROBIOLOGY | Applied and Environmental Microbiology®

BIOTECHNOLOGY

Functional Characterization of a 28-Kilobase Catabolic Island from *Pseudomonas* sp. Strain M1 Involved in Biotransformation of β-Myrcene and Related Plant-Derived Volatiles

Pedro Soares-Castro,[a] Pedro Montenegro-Silva,[a] Hermann J. Heipieper,[b] Pedro M. Santos[a]

CBMA—Centre of Molecular and Environmental Biology, Department of Biology, University of Minho, Braga, Portugal[a]; Helmholtz Centre for Environmental Research-UFZ, Department of Environmental Biotechnology, Leipzig, Germany[b]

ABSTRACT *Pseudomonas* sp. strain M1 is able to mineralize highly hydrophobic and recalcitrant compounds, such as benzene, phenol, and their methylated/halogenated derivatives, as well as the backbone of several monoterpenes. The ability to use such a spectrum of compounds as the sole carbon source is, most probably, associated with a genetic background evolved under different environmental constraints. The outstanding performance of strain M1 regarding β-myrcene catabolism was elucidated in this work, with a focus on the biocatalytical potential of the β-myrcene-associated core code, comprised in a 28-kb genomic island (GI), predicted to be organized in 8 transcriptional units. Functional characterization of this locus with promoter probes and analytical approaches validated the genetic organization predicted *in silico* and associated the β-myrcene-induced promoter activity to the production of β-myrcene derivatives. Notably, by using a whole-genome mutagenesis strategy, different genotypes of the 28-kb GI were generated, resulting in the identification of a novel putative β-myrcene hydroxylase, responsible for the initial oxidation of β-myrcene into myrcen-8-ol, and a sensor-like regulatory protein, whose inactivation abolished the *myr*$^+$ trait of M1 cells. Moreover, it was demonstrated that the range of monoterpene substrates of the M1 enzymatic repertoire, besides β-myrcene, also includes other acyclic (e.g., β-linalool) and cyclic [e.g., *R*-(+)-limonene and (−)-β-pinene] molecules. Our findings are the cornerstone for following metabolic engineering approaches and hint at a major role of the 28-kb GI in the biotransformation of a broad monoterpene backbone spectrum for its future biotechnological applications.

IMPORTANCE Information regarding microbial systems able to biotransform monoterpenes, especially β-myrcene, is limited and focused mainly on nonsystematic metabolite identification. Complete and detailed knowledge at the genetic, protein, metabolite, and regulatory levels is essential in order to set a model organism or a catabolic system as a biotechnology tool. Moreover, molecular characterization of reported systems is scarce, almost nonexistent, limiting advances in the development of optimized cell factories with strategies based on the new generation of metabolic engineering platforms. This study provides new insights into the intricate molecular functionalities associated with β-myrcene catabolism in *Pseudomonas*, envisaging the production of a molecular knowledge base about the underlying catalytic and regulatory mechanisms of plant-derived volatile catabolic pathways.

KEYWORDS *Pseudomonas*, biotransformation, monoterpenes, genomic island, promoter probes, β-myrcene hydroxylase

Received 11 November 2016 **Accepted** 14 February 2017

Accepted manuscript posted online 17 February 2017

Citation Soares-Castro P, Montenegro-Silva P, Heipieper HJ, Santos PM. 2017. Functional characterization of a 28-kilobase catabolic island from *Pseudomonas* sp. strain M1 involved in biotransformation of β-myrcene and related plant-derived volatiles. Appl Environ Microbiol 83:e03112-16. https://doi.org/10.1128/AEM.03112-16.

Editor Maia Kivisaar, University of Tartu

Address correspondence to Pedro M. Santos, psantos@bio.uminho.pt.

Plant monoterpenes and their derivatives are widely used in industry processes because of their organoleptic and therapeutic properties (1–4). Among them, β-myrcene (7-*methyl*-3-methylene-1,6-octadiene) is one of the most promising monoterpenes, being used mainly as starting material for the chemical synthesis of value-added products with a broad spectrum of applications, including pharmaceutics (e.g., antimutagenics, analgesics, tyrosinase inhibitors) and top-selling flavors and fragrances (e.g., linalool, nerol, geraniol, citral, menthol), (4) and also in the production of polymers, biodegradable surfactants, pheromones, and agrochemicals (4–6). The intrinsic physicochemical properties of monoterpene molecules (e.g., high hydrophobicity and structural instability) pose challenges regarding their utilization in industrial catalysis. Their catalytic modification to obtain oxidized/hydroxylated monoterpene derivatives usually requires the presence of a second phase of organic solvents or utilization of detergents to aid mass transfer in catalytic processes (5–7). Strikingly, biological systems can overcome the limited availability of substrate and quickly adapt to the hydrophobic character of monoterpenes, with the advantage of yielding "natural" derivatives with high regio- and stereoselectivity (6, 8). Moreover, the versatility of microorganisms allows easy and inexpensive maintenance of the biocatalyst, whose catalytic machinery can be improved and optimized by modern metabolic engineering platforms, allowing limitless possibilities of novel products and industrial applications (9, 10).

Pseudomonas sp. strain M1 is so far the best investigated aerobic bacteria able to mineralize β-myrcene (11–13), as well as to oxidatively transform β-citronellol and citral (14). Strain M1 has been previously characterized, using a systems biology approach, at the genome, transcriptome, and proteome levels (12, 13). The sequencing of the genome of strain M1 and characterization of the myrcene stimulon by transcriptome sequencing (RNA-seq) identified a novel 28-kb genomic island (GI), whose expression was strongly stimulated in the presence of β-myrcene. This locus includes genes, apparently organized in eight transcriptional units (TUs), whose products are putatively involved in (i) substrate sensing, (ii) gene expression regulation, and (iii) β-myrcene oxidation and bioconversion of β-myrcene derivatives into the central metabolism intermediates (12). Significantly, the majority of the functional modules present in the 28-kb β-myrcene-inducible catabolic island did not show high homology with sequences available in databases and seemed to have evolved through the assembly of several functional blocks acquired from different bacteria, probably at different evolutionary stages and driven by particular niche-related constraints (12). Moreover, the molecular characterization of reported microbial enzymatic systems involved in the catabolism of monoterpenes is scarce, almost nonexistent, limiting advances in the development of tailored cell factories. The work presented here is the first report of the functional characterization of the 28-kb GI associated with the catabolism of β-myrcene, by using molecular and analytical approaches during biotransformation experiments with *Pseudomonas* sp. M1 strains harboring different mutations within the genomic island. Most importantly, a novel putative β-myrcene hydroxylase and a sensor-like regulatory protein were identified, and insights into the substrate range of the 28-kb GI were provided, thus describing the biotechnological potential of M1 enzymatic machinery for the biotransformation of a broader range of acyclic and cyclic plant-derived volatiles.

RESULTS

Pseudomonas sp. M1 is able to mineralize β-myrcene, with the catabolic genetic core code being located on a 28-kb GI (12). The biotechnological exploitation of its functional modules requires a detailed understanding of which genes are directly involved in β-myrcene catabolism, their interactions, and regulation. As described by Soares-Castro and Santos (12), the β-myrcene-inducible 28-kb GI was predicted *in silico* to be organized in eight TUs, whose putative encoded products are summarized in Table 1. TU1, TU3, TU5, TU6, and TU7 are predicted to mainly comprise catabolic genes, TU4 and

TABLE 1 Correspondence between genes comprising the β-myrcene-inducible 28-kb GI in *Pseudomonas* sp. M1 and promoter regions and transcriptional units predicted *in silico*[a]

Locus tag	Predicted product	Promoter/TU
PM1_0216305	CoA dehydrogenase	P1/TU1
PM1_0216310	CoA dehydrogenase	P1/TU1
PM1_0216315	CoA acetyltransferase	P1/TU1
PM1_0216320	Sensory transducer	P2/TU2
PM1_0216325	Membrane protein	P2/TU2
PM1_0216330	CoA acetyltransferase	P3/TU3
PM1_0216335	Monooxygenase	P3/TU3
PM1_0216340	Oxidoreductase	P3/TU3
PM1_0216345	CoA dehydrogenase	P3/TU3
PM1_0216350	Epoxide hydrolase	P3/TU3
PM1_0216355	Hypothetical protein	P3/TU3
PM1_0216360	LuxR family transcriptional regulator	P4/TU4
PM1_0216365	Rubredoxin	P5/TU5
PM1_0216370	Fatty acid desaturase	P5/TU5
PM1_0216375	LuxR family transcriptional regulator	P6/TU6
PM1_0216380	Oxidoreductase	P6/TU6
PM1_0216385	CoA synthetase MyrC	P6/TU6
PM1_0216390	Alcohol dehydrogenase MyrB	P6/TU6
PM1_0216395	Aldehyde dehydrogenase MyrA	P6/TU6
PM1_0216400	CoA hydratase	P7/TU7
PM1_0216405	LysR family transcriptional regulator	P8/TU8
PM1_0216410	Hypothetical protein	P8/TU8

[a]Promoter regions and transcriptional units were predicted *in silico* by Soares-Castro and Santos (12).

TU8 are predicted to encode regulatory elements, and the TU2 is predicted to encode a chemosensory system.

Reporter systems validate the promoter regions controlling β-myrcene-dependent operons from the 28-kb genomic island. The promoter regions from each TU, listed in Table 1, were cloned into the promoter probe vector pSEVA637, envisaging the validation of the previously predicted promoter segments (12) and, therefore, detailing the operonic organization of the genomic island (Fig. 1).

As depicted in Fig. 1, promoter regions P1, P2, P3, P5, P6, and P7 showed a β-myrcene-dependent production of green fluorescent protein (GFP) in M1 cells, validating these DNA segments as functional elements and the overall modular organization of the island. The promoter fusions of P4 and P8 presented low inducible activity (<1.5-fold increase) under the tested conditions and, thus, were excluded from the following analysis.

To better understand the role and functional interplay between the enzymatic systems encoded by the 28-kb GI of M1 strain and to obtain insights regarding the underlying regulatory mechanism, the expression of the putative chemosensory genetic cluster TU2 was inactivated using a whole-genome mutagenesis strategy, by using the random transposon pBAM1 harboring the reporter fusion P2::GFP to target its potential activators. Both genomic and transposon-borne P2 promoters would be activated and the fluorescent reporter would be expressed if the transposon harboring P2::GFP was inserted into a neutral locus. Alternatively, if a transposition event interrupted a locus essential for the activation of promoter P2 (and TU2), the reporter would not be induced, resulting in nonfluorescent cells. The mutagenesis approaches created different M1-derived genotypes, targeting genes within the 28-kb GI, with the M1-C19 strain showing the insertion of the P2::GFP reporter transposon cassette in *PM1_0216375* and the M1-C38 strain showing the insertion of the P2::GFP reporter transposon cassette in *PM1_0216370*.

Mutant strains show different growth kinetics when β-myrcene is supplemented as the sole carbon source. In this work, three mutants of strain M1 showing phenotypic alterations regarding β-myrcene catabolism were characterized: M1-N22 (11), M1-C19, and M1-C38. M1 wild type (wt) and derived strains were grown in minimal medium (MM) supplemented with β-myrcene as the sole carbon source

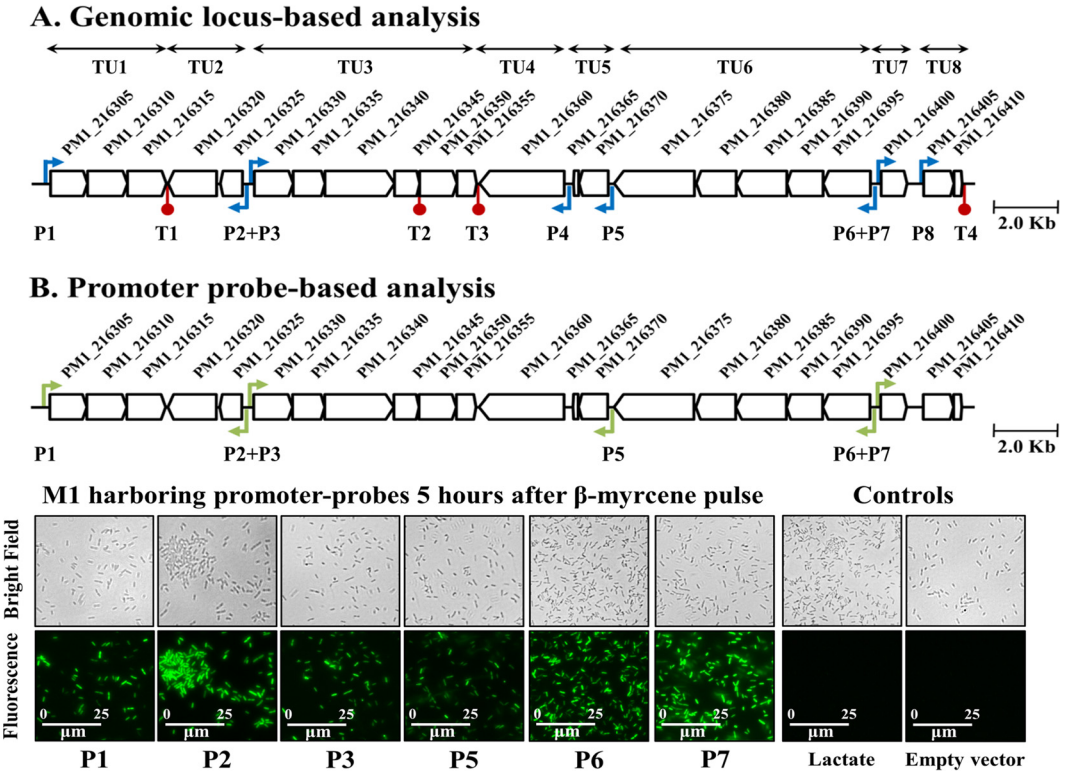

FIG 1 Operonic organization of the newly identified 28-kb GI harboring the β-myrcene core code, predicted *in silico* by Soares-Castro and Santos (12) (A) and validated by promoter reporters (B). Genes are organized in transcriptional units (TUs), promoter regions (P) are illustrated by blue/green arrows, and terminator sites are depicted as red circles. Microscopy images correspond to a total magnification of ×400. Controls of promoter induction are shown for P2 and are representative of the absence of fluorescence in all reporters. Cultures of M1 wt cells harboring pSEVA637 constructs were supplemented with 48 mM lactate or 47.8 μmol of β-myrcene in solution.

to assess the effect of the different 28-kb GI genotypes in the catabolic pathway of β-myrcene (see Fig. S1 in the supplemental material).

In the wt strain, β-myrcene supports an increase in the culture optical density and is accompanied by a decrease in culture pH, derived from the oxidation of β-myrcene in acidic derivatives and the channeling of intermediates to the central metabolism (13). Thus, the decrease in pH observed at the initial time points for M1-N22 suggested a partial catabolism of the β-myrcene backbone in this mutant, despite the residual increase in the optical density values. The M1-N22 strain harbors an insertion of a mini-Tn*5*-Km transposon in the *myrB* gene (*PM1_0216390*), which encodes an alcohol dehydrogenase. Iurescia et al. (11) isolated the M1-N22 mutant as a β-myrcene-negative strain, in which a myrcene alcohol, myrcen-8-ol, was accumulated instead of proceeding to mineralization. The initial β-myrcene-supported growth of M1-N22 cells was significantly compromised, in comparison with that of the M1 wt strain, due to the disruption of the predicted sequential oxidation of the β-myrcene molecule (β-myrcene ≫ myrcene alcohol ≫ myrcene aldehyde ≫ myrcene acid). Nonetheless, in this work, the M1-N22 strain was able to resume growth in liquid cultures supplemented with β-myrcene as the sole carbon source and reached optical densities similar to that of the wt strain within 48 h of growth. In contrast, the M1-C19 and M1-C38 mutants were not able to grow in β-myrcene as the sole carbon source within the sampled time (growth was extended to 5 days without an increase in the optical density or a decrease in pH values).

The profile of promoter activity in M1-derived strains shows different β-myrcene-induced enzymatic repertoires. Further molecular analysis was carried out to describe the effect of mutations on the overall expression of the 28-kb GI and to link the specific

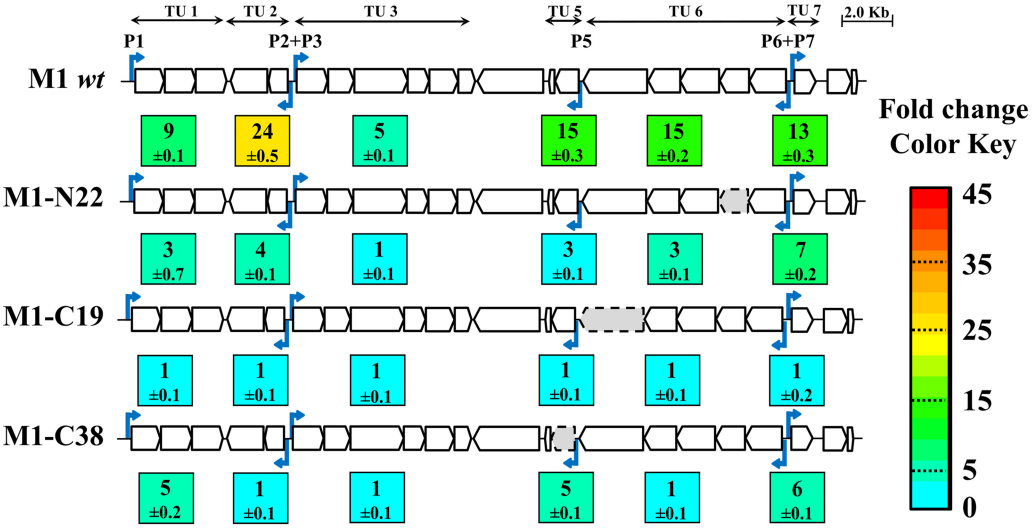

FIG 2 Overview of the promoter activity of the 28-kb genomic island in M1 wt and mutant strains, obtained from whole-genome mutagenesis. M1 strains harbored the reporter pSEVA637, fused to each one of the six validated promoter regions (P1, P2, P3, P5, P6, P7). Cells were grown in MM with 48 mM lactate, and GFP fluorescence was measured after 5 h of supplementation with 9.6 μmol of β-myrcene. The heatmap (colored squares aligned with predicted TUs) indicates the variation in fold induction of the GFP reporter for promoters, in the presence or absence of β-myrcene in the culture medium, as the myrcene/lactate ratio of relative light units normalized to the optical density of the culture. The knockout of genes or cluster of genes is shown for each mutant by gray shading and a dotted line: disruption of *PM1_0216390* (encoding the alcohol dehydrogenase MyrB) in M1-N22 by transposon insertion; disruption of *PM1_0216375* (coding for a regulatory protein from the LuxR family) in M1-C19 by transposon insertion; disruption of *PM1_0216370* (encoding a fatty acid desaturase) in M1-C38 by transposon insertion.

activity of its functional modules to key enzymatic steps of the β-myrcene catabolic pathway.

To understand the effect of the three mutations in the activity of the different transcriptional units within the 28-kb island, during β-myrcene induction, the pSEVA637 probes harboring the validated promoters were mobilized to M1-N22, M1-C19, and M1-C38 cells. The fluorescence of the wt and mutant strains was measured after 5 h of β-myrcene pulse in lactate-growing cultures (Fig. 2).

Although M1-C19 and M1-C38 strains were not able to use β-myrcene as the sole carbon source at the sampled time points in growth kinetics experiments, their promoter activity profiles within the GI were slightly different from each other. The disruption of the putative LuxR transcriptional regulator PM1_0216375 in M1-C19 switched off all the promoters assayed (hence supporting the inability to mineralize β-myrcene), as the ratio of fluorescence levels in the presence and absence of β-myrcene was approximately 1. Therefore, *PM1_0216375* was shown to code for a primary activator of the β-myrcene-induced catabolic machinery. The disruption of the putative PM1_0216370 in M1-C38 only resulted in the inactivation of promoters P2, P3, and P6, whereas promoters P1, P5, and P7 remained active but were downregulated approximately 2-fold, 3-fold, and 2-fold, respectively. The loss of the *myr*$^+$ phenotype associated with the inactivation of the GI promoter activity in M1-C38 strongly indicated that PM1_0216365 to PM1_0216370 (TU5) is essential for β-myrcene catabolism. In agreement, complementation of strains M1-C19 and M1-C38 with PM1_0216375 and TU5 sequences, respectively, under the control of the inducible *xylS*-P*m* system, restored the ability of both mutants to grow in MM supplemented with β-myrcene in the presence of the inducer 3-methylbenzoate (data not shown).

In strain M1-N22, interruption of myrcene alcohol oxidation into myrcene aldehyde led to an overall reduction in the reporter levels. The activities of promoters P1, P2, P5, P6, and P7 were reduced approximately 3-fold, 6-fold, 6-fold, 5-fold, and 2-fold, respectively, whereas the promoter P3 remained inactive.

Biotransformation of β-myrcene correlates with the expression of promoter reporters. To validate the role of the functional modules from the 28-kb GI, the

TABLE 2 Metabolites identified in β-myrcene ($C_{10}H_{16}$) biotransformation experiments with the M1 wt strain[a]

Predicted metabolite ID (formula) (compound no.)	Area (%) based on GC-MS[b]							
	M1 (wt)		M1-N22		M1-C19		M1-C38	
	0.5 h	3.5 h	0.5 h	3.5 h	0.5 h	3.5 h	0.5 h	3.5 h
Myrcenal ($C_{10}H_{14}O$) (1)	0.8 ± 0.2	1.8 ± 0.4	ND	ND	ND	ND	ND	ND
Myrcen-8-ol ($C_{10}H_{16}O$) (2)	9.0 ± 3.6	6.0 ± 1.3	14	50 ± 10	ND	ND	ND	ND
4-Methylhexanoic acid ($C_7H_{14}O_2$) (3)	ND	0.4 ± 0.3	ND	ND	ND	ND	ND	ND
4-Methyl-3-hexenoic acid ($C_7H_{12}O_2$) (4)	ND	1.3 ± 0.2	ND	ND	ND	ND	ND	ND
Myrcenoic acid ($C_{10}H_{14}O_2$) (5)	0.4 ± 0.2	17 ± 0.6	0.1	5.8 ± 0.3	ND	ND	ND	ND

[a]The effect of the different genotypes of the mutant strains is compared to the profile of the wt cells. A detailed characterization of the detected metabolites is shown in Table S2 and Fig. S2 in the supplemental material.

[b]Peak areas from identified metabolites normalized as a percentage of the total area of the chromatogram, shown as average values ± standard deviation when replicates were available, at 30 min and 3.5 h of β-myrcene biotransformation. ND, not detected in any replicate.

metabolites from β-myrcene biotransformation experiments were identified and the cell membrane response to the hydrophobicity of β-myrcene was characterized in the different M1 strains.

Metabolites of β-myrcene biotransformation experiments with the M1 wt and derived strains were identified by gas chromatography coupled to mass spectrometry (GC-MS). M1 cells were grown in mineral medium supplemented with 48 mM lactate, to which β-myrcene was added at mid-exponential phase of growth. The supernatants were collected at early and late stages of the monoterpene catabolism (30 min and 3.5 h), and the β-myrcene derivatives from culture supernatants were identified by GC-MS (Table 2; detailed in Table S2 and Fig. S2).

Table 2 lists the metabolites identified from β-myrcene biotransformation in the M1 wt strain and compares them with the profile of mutant strains. The relative quantification was calculated based on their peak area, normalized as the percentage of the total spectral area of the chromatogram (15, 16), which allows one to infer differences in metabolite abundances between peaks of the same chromatogram and, to some extent, between peaks of different samples (17).

In all wt cultures assayed after 30 min of β-myrcene pulse, the major metabolite detected (compound 2, retention index of 1,920) was identified as myrcen-8-ol. Although this compound was not available in the databases used for data mining, the obtained mass spectrum matched the mass spectrum of the detected alcohol and the synthetic myrcen-8-ol standard published previously (11), described as the substrate for the alcohol dehydrogenase MyrB. As shown by searching the mass spectrum of myrcen-8-ol, metabolite databases do not comprise a large number of myrcene-derived compounds in a mass spectrum search, reflecting the lack of knowledge available regarding β-myrcene catabolic pathways, which in turn reduced the rate of metabolite identification.

A putative C_{10} aldehyde (compound 1, retention index of 1,708) and carboxylic acid (compound 5, retention index of 2,466) were also detected 30 min after addition, which most likely resulted from the oxidation of the terminal hydroxyl group of myrcen-8-ol, mediated by the alcohol dehydrogenase MyrB and the aldehyde dehydrogenase MyrA. An unequivocal identification of compounds 1 and 5 was also not possible using the available databases. Nevertheless, the comparison of the mass spectrum of compound 5 to the mass spectrum of the 2-*methyl*-6-methylen-2,7-octadienoic acid methyl ester, reported by Narushima et al. (18) from supernatants of *Pseudomonas* sp. strain S4-2, supported its identification as 2-*methyl*-6-methylen-2,7-octadienoic acid (myrcenoic acid). Moreover, the detection of mass peaks 53, 67, and 93 in the *m/z* spectra of compounds 1 and 5, easily inferred by predicting the fragmentation pattern of the β-myrcene-like backbone and common to myrcen-8-ol, supported the identification of the two derivatives as myrcene aldehyde and myrcenoic acid, respectively. Although not present in all assayed supernatants, two putative derivatives of the predicted myrcenoic acid were detected in M1 wt supernatants at 3.5 h of biotransformation: 4-methyl-3-hexenoic acid (compound 4, retention index of 2,045)

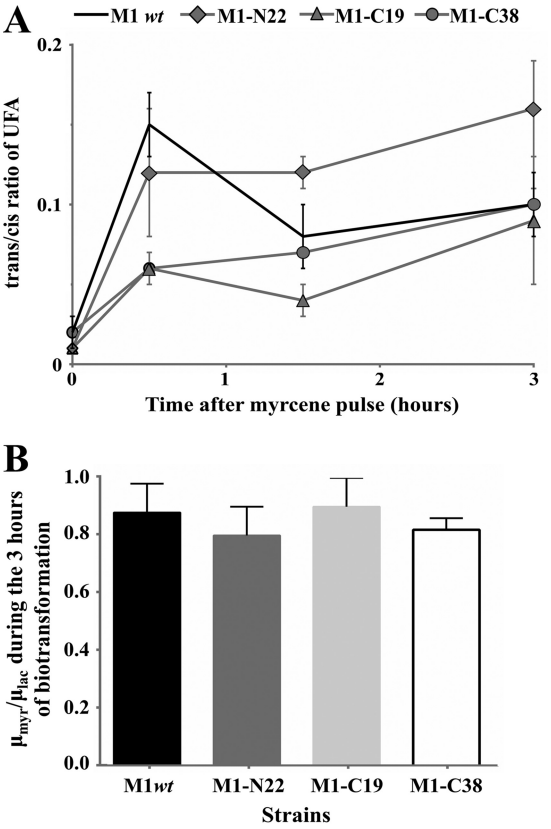

FIG 3 Effect of β-myrcene exposure on the membrane fatty acid content (A) and cell viability (B) of M1 and derived strains. (A) The membrane adaptive response, with respect to the *trans*/*cis* ratio of unsaturated acyl chains (UFA), was analyzed by GC of fatty acid methyl esters, at 0.5 h, 1.5 h, and 3 h after supplementation with a saturating amount of β-myrcene, in three independent experiments. Kinetics of strain M1 is shown in black, whereas that of M1 mutants is shown in gray: M1-N22 derived from the interruption of the alcohol dehydrogenase MyrB (◆), M1-C19 derived from the interruption of the transcriptional regulator PM1_0216375 (▲), M1-C38 derived from the interruption of the putative myrcene hydroxylase PM1_0216370 (●). (B) The number of cells as CFU was quantified during the same time range employed to assess cell viability. The specific growth rate for each strain growing in lactate (μ_{lac}) or lactate with β-myrcene pulse (μ_{myr}), during the 3 h assayed, was calculated and expressed as a ratio of μ_{myr} to μ_{lac}.

and 4-methylhexanoic acid (compound 3, retention index of 1,925). The former was suggested by Narushima et al. (18) to be a product of a β-oxidation-like catabolic step targeting the myrcenoic acid, with subsequent elimination of the carboxyl-containing C_3 unit as propionyl-coenzyme A (propionyl-CoA), whereas the latter might result from the dehydrogenation of the C-3,C-4 double bond of 4-methyl-3-hexenoic acid.

Similar to what was reported by Iurescia et al. (11), the disruption of *myrB* in strain M1-N22 led to the early accumulation of the identified myrcen-8-ol, with a concomitant loss of the ability to produce the putative myrcene aldehyde (compound 1) or the 4-methyl-3-hexenoic acid (compound 4), not detected in supernatants of this mutant. Neither strain M1-C19 nor M1-C38 produced any of the metabolites proposed for the catabolic pathway.

The different GI genotypes were also translated into different physiological traits at the membrane level. Since hydrophobic molecules are expected to be membrane-active compounds (19, 20), changes in the membrane lipid profile and cell viability were analyzed when M1 and derived strains were exposed to saturating amounts of β-myrcene. Cells were sampled and fatty acid methyl esters (FAMEs) were analyzed by gas chromatography (Fig. 3) in cometabolism experiments by using lactate as the primary carbon source. Control cells grown solely with lactate were collected at the same time points of FAME analysis, before β-myrcene supplementation and corresponding to 3 h after monoterpene exposure.

The major changes observed in all M1 strains after β-myrcene supplementation were associated with the *cis*-to-*trans* isomerization of $C_{16:1}$ and $C_{18:1}$ unsaturated fatty acids (Fig. 3A). Whereas the *trans/cis* ratio in both controls was approximately 0.02, these values increased up to 8-fold after 30 min of β-myrcene pulse in the assayed strains (from a ratio of 0.06 in M1-C19 and M1-C38 to a ratio of >0.1 in M1 wt and M1-N22 strains). This change in the content of membrane lipids coincided with the production of myrcen-8-ol in the wt strain (and accumulation in M1-N22), as depicted in Table 2. In contrast, the *myr*-negative M1-C19 and M1-C38 strains showed the lowest increase in *trans/cis* ratios, most probably due to the presence of β-myrcene alone, since the extensive downregulation of the 28-kb GI promoters/TUs impaired the successful biotransformation and utilization of β-myrcene to support cell growth.

M1 cells were able to rapidly adapt to the hydrophobic properties of β-myrcene and to the overaccumulation of monoterpene derivatives as a proficient biocatalyst, in which significant inhibitory effects were not detected in cell viability (Fig. 3B).

The LuxR family transcriptional regulator PM1_0216375 is a key activator of the enzymatic machinery encoded by the 28-kb GI. As indicated by previous results, PM1_0216375 is an essential activator of the β-myrcene-inducible 28-kb GI. Moreover, the role of the two other putative transcriptional regulators, PM1_0216360 and PM1_0216405, encoded in this locus remained undetermined. As depicted in Fig. 4, both PM1_0216360 and PM1_0216375 belong to the LuxR family, included in the MalT subfamily, although the percentages of amino acid identity with the closest homologs in the NCBI nonredundant protein database are only 46% (from *Burkholderia* sp. strain MSh2; GenBank accession no. WP_063934625.1) and 28% (from *Polycyclovorans algicola*; GenBank accession no. WP_029891500.1), respectively. PM1_0216405 is a member of the LysR family (Fig. 4), with 83% of amino acids shared with a putative regulator from *Pseudomonas aeruginosa* (GenBank accession no. WP_023104498.1).

Similar to the MalT-like regulators, PM1_0216375 is a large protein (872 amino acids [aa]), harboring three main functional domains (Fig. 4). The protein domains depicted in Fig. 4 are well described in MalT from *Escherichia coli* K-12 and confer a one-component switch-like function to the protein. The ATPase domain comprises a conserved nucleotide oligomerization domain, which alternates between resting (ADP-bound) and active (ATP-bound) conformations, being required for the oligomerization of the regulator into a protein complex. The sensor domain is responsible for the recognition of the inducer metabolite in MalT (21). The interaction with the inducer and ATP results in conformational changes in the MalT regulator (22), which allow the effector domain (winged helix-turn-helix [WHTH]) to bind the recognition site and activate transcription (22). Although not so extensively characterized, the MalT-like AcoK regulator is hypothesized to use a slightly different mechanism of regulation. In contrast to MalT, the ATPase domain in AcoK mutants appeared to not be essential for efficient recognition of the DNA-binding site. AcoK was hypothesized to bind the regulated DNA prior to interacting with the ATP or inducer, although both molecules were still essential for a conformational switch between an inactive and an active form (23).

The amino acid identities between the functional domains of PM1_0216375 and other characterized MalT-like regulators are shown in Table S3 in the supplemental material, with the respective sequence alignments shown in Fig. S3, S4, and S5. Despite the low identity levels observed between the predicted domains of PM1_0216375 and the MalT, AcoK, and AlkS regulators, the conservation of key motifs, such as the Walker A and B motifs involved in ATPase activity, suggests similar mechanisms of transcriptional activation in the presence of β-myrcene.

PM1_0216370 is more closely related to hydroxylases than fatty acid desaturases and probably catalyzes the terminal hydroxylation of the β-myrcene backbone. The predicted TU5 codes for an oxidoreductase system, composed of two genes whose products are annotated as a putative fatty acid desaturase (PM1_0216370) and a rubredoxin (PM1_0216365). The loss of the ability to use β-myrcene as the sole carbon source in strain M1-C38 (Fig. 2; Fig. S1) indicated that TU5, namely, the

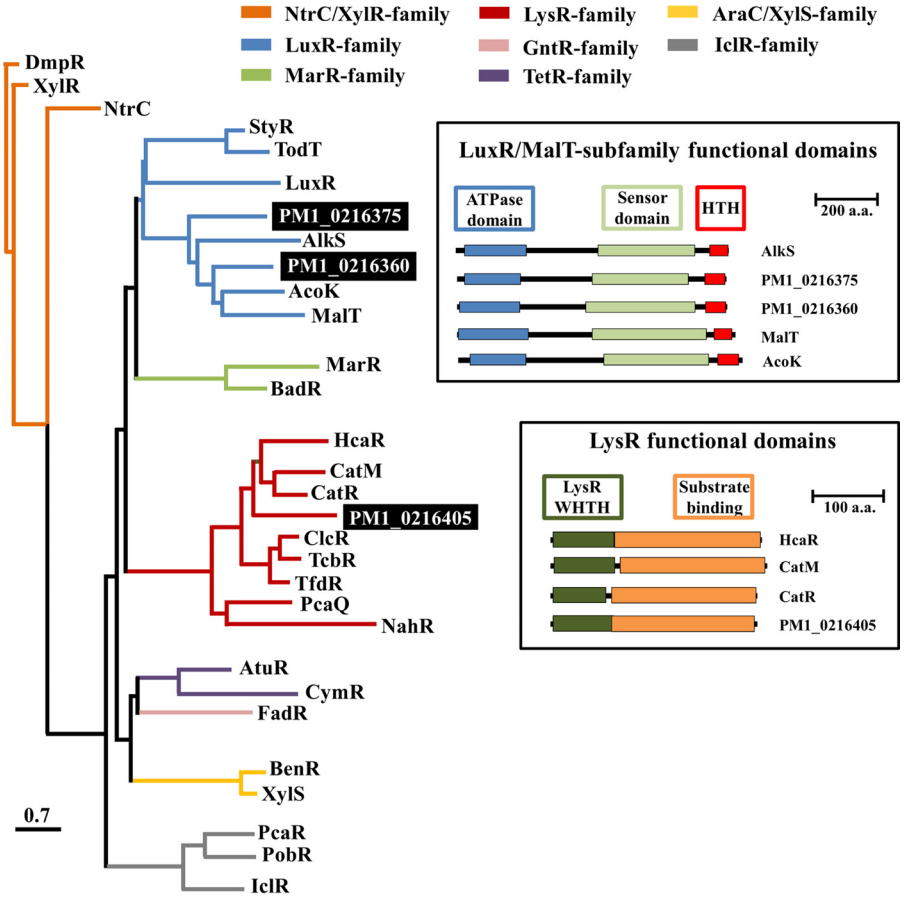

FIG 4 Homology of the three putative regulators encoded by the *β*-myrcene-inducible 28-kb GI of strain M1. The eight major families of transcriptional regulators involved in the catabolism of acyclic and cyclic/aromatic hydrocarbons are depicted in different-colored branches. The regulators PM1_0216360, PM1_0216375, and PM1_0216405 are highlighted by a black box. The alignment of protein sequences was performed with MAFFT to generate the unrooted tree. A schematic representation of the protein domains predicted by InterPro for the PM1_0216360, PM1_0216375, and PM1_0216405 protein sequences, as well as for other characterized members of the respective families of regulators, is shown. ATPase, nucleotide-binding oligomerization domain; WHTH/HTH, helix-turn-helix domain; a.a., amino acid residues. The UniProt accession numbers of the sequences used are as follows: AcoK, Q48411; AlkS, P17051; AtuR, Q9HZW2; BadR, O07458; BenR, Q4K9X4; CatM, P07774; CatR, P20667; ClcR, Q05840; CymR, O33453; DmpR, Q06573; FadR, P0A8V6; HcaR, Q47141; IclR, P16528; LuxR, P35327; MalT, P06993; MarR, P27245; NahR, P10183; NtrC, P10577; PcaQ, P0A4T6; PcaR, I7C334; PobR, Q43992; StyR, O30989; TcbR, P27102; TfdR, Q46M57; TodT, I7CA98; XylR, P06519; and XylS, P07859.

PM1_0216370 gene, plays an essential role in the catabolic pathway. The PM1_0216370 protein shared only 52% amino acid identity with its closest homolog from the NCBI nonredundant protein database (fatty acid desaturase from *Novosphingobium* sp. strain AAP93, GenBank accession no. WP_054123145.1). Moreover, a detailed inspection of the protein sequence of PM1_0216370 predicted that the enzyme might fold into several transmembrane helix domains (5 or 6 domains predicted *in silico* by several tools in Fig. S6) and contains three histidine-rich motifs, highly conserved in proteins of the membrane nonheme di-iron family: $HX_{3-4}H$, $HX_{2-3}HH$, and HXXHH. The conservation of the histidine-rich motifs is shown in Fig. 5A (protein alignment shown in Fig. S7), which are described to be required for iron binding and for the oxidative enzyme activity (24). The nonheme di-iron family of proteins comprises not only membrane fatty acid desaturases but also membrane hydroxylases/monooxygenases (e.g., alkane 1-monooxygenase AlkB, xylene monooxygenase XylM, *p*-cymene monooxygenase CymAa) (24), as shown in Fig. 5A.

Furthermore, both the protein alignment (Fig. 5A; Fig. S7) and the homology-based clustering in Fig. 5B showed that PM1_0216370 shared higher sequence homology

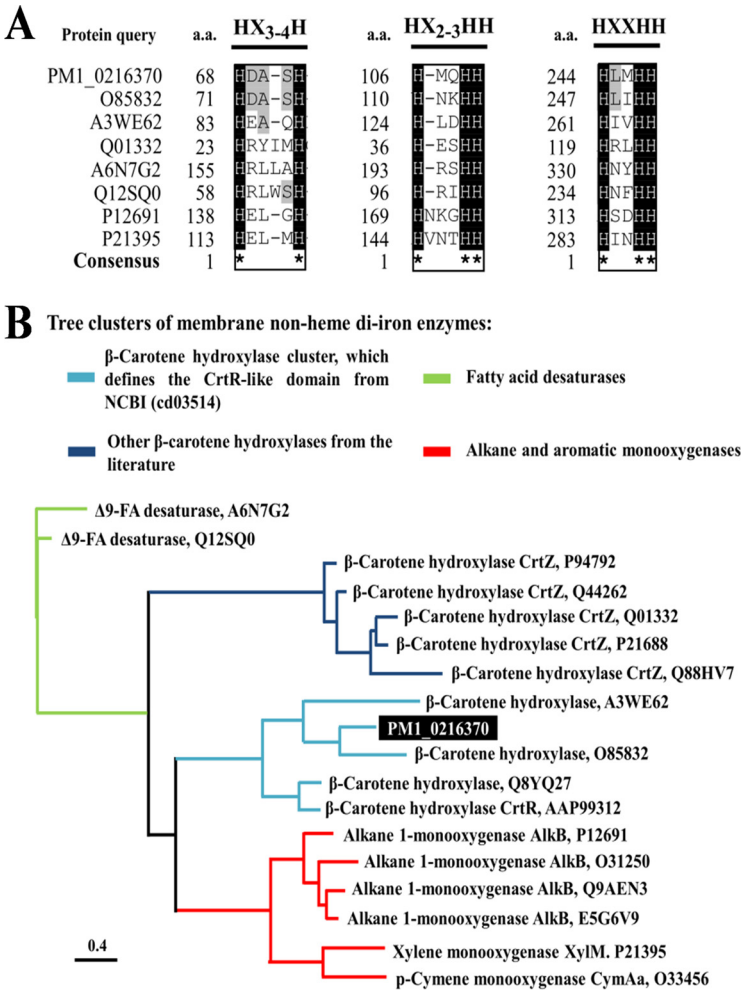

FIG 5 Conservation of the histidine-rich motifs $HX_{3-4}H$, $HX_{2-3}HH$, and HXXHH in β-myrcene-induced PM1_0216370 (A), common to all membrane nonheme hydroxylases, monooxygenases, and fatty acid desaturases, described by Shanklin and Whittle (24). Asterisks indicate positions which have single, fully conserved residues (black). Residues conserved between the query sequences and PM1_0216370 are highlighted in gray. The numbering of each sequence represents the position of each residue in the original protein sequence. (B) The homology-based analysis of the *PM1_0216370* gene product (highlighted by a black box in panel A), annotated as a fatty acid desaturase, is shown. Protein sequences of PM1_0216370 and other reported membrane nonheme di-iron enzymes were aligned using MAFFT, and the protein region comprising the three characteristic histidine-rich motifs was used to generate the unrooted tree. The accession numbers of the protein sequences retrieved from UniProt are indicated.

with the β-carotene hydroxylases (Fig. 5B, light blue), whose amino acid identity considering their complete protein sequences ranged from 41% to 22%. The alignment of PM1_0216370 with protein sequences of the other tree clusters registered identity values below 15%. Therefore, *PM1_0216370* might code for the β-myrcene monooxygenase, not identified in previous studies, which putatively catalyzes the first enzymatic step of the β-myrcene catabolic pathway and conversion to myrcen-8-ol.

M1 cells are able to biotransform different cyclic and acyclic monoterpenes. Previous reports regarding biotransformation of plant-derived volatiles by *Pseudomonas* sp. M1 have described solely the utilization of β-myrcene, β-citronellol, and citral as carbon sources (13, 14). To further evaluate the biotechnological potential of the M1 enzymatic repertoire for other plant volatiles, biotransformation experiments were performed with wt cells by supplementing lactate-growing cultures with other acyclic (linalyl acetate) and cyclic [*R*-(+)-limonene and (−)-β-pinene] monoterpenes. After monoterpene supplementation, the metabolite profile of culture supernatants was identified by GC-MS (Table 3; detailed in Table S4 and Fig. S8).

TABLE 3 Metabolites identified in biotransformation experiments with M1 wt[a]

Identified peak (RI)[b]	Predicted ID	Formula	ID method[b]
Linalyl acetate ($C_{12}H_{20}O_2$)			
1,552	β-Linalool	$C_{10}H_{18}O$	MS, RI, Std
1,852	Geraniol	$C_{10}H_{18}O$	MS, RI, Std
2,342	Geranic acid	$C_{10}H_{16}O_2$	MS, RI, Std
Limonene ($C_{10}H_{16}$)			
2,287	Limonene-1,2-diol	$C_{10}H_{18}O_2$	MS, RI
β-Pinene ($C_{10}H_{16}$)			
1,703	α-Terpineol	$C_{10}H_{18}O$	MS, RI, Std
2,249	Citronellic acid	$C_{10}H_{18}O_2$	MS, RI

[a]The M1 wt strain was grown in MM supplemented with 48 mM lactate and acyclic [linalyl acetate and (±)-β-citronellol] or cyclic [*R*-(+)-limonene and (−)-β-pinene] monoterpenes. A detailed characterization of the detected metabolites is shown in Table S4 and Fig. S8 in the supplemental material.
[b]RI, retention index; MS, mass spectrum search; Std, validation with pure standard.

Supplementation with linalyl acetate resulted in the identification of linalool (retention index of 1,552), geraniol (retention index of 1,852) and geranic acid (retention index of 2,342) by correspondence of mass spectra and retention indices. Strain M1 was also able to hydroxylate the cyclic structure of *R*-(+)-limonene into limonene-1,2-diol (retention index of 2,287), and (−)-β-pinene biotransformation experiments resulted in the identification of α-terpineol (retention index of 1,703) and citronellic acid (retention index of 2,249) in culture supernatants.

In order to determine the potential involvement of the 28-kb GI from strain M1 in the enzymatic oxidation of other monoterpene backbones, the reporter activity of the GFP-based promoter probes was evaluated in the presence of different plant-derived volatiles.

The 28-kb GI promoters are responsive to other plant-derived volatiles. Besides β-myrcene, the acyclic linalyl acetate, (±)-β-citronellol, and geraniol and the cyclic *R*-(+)-limonene, (−)-carveol, (−)-α-terpineol, and (−)-β-pinene were used as potential inducers. The promoter activity is shown in Fig. 6, measured as fold induction between the GFP levels detected in lactate-grown cells challenged with a monoterpene and those in cells grown with lactate as the sole carbon source (control cultures).

Under the tested conditions, all promoter regions assayed showed higher induction levels in the presence of β-myrcene, confirming this substrate as the more effective enhancer of the 28-kb genomic island (Fig. 6A).

The 28-kb GI was responsive to other monoterpene backbones, although an induction pattern related to the structure of the molecule was not apparent (Fig. 6B). Of the acyclic monoterpenes tested, geraniol activated promoter P6 by 4-fold, P2 by approximately 3-fold, and P1 and P7 by 2-fold. Supplementation with linalyl acetate increased the GFP levels of P2 reporter by 3-fold and of P6 and P7 by approximately 2-fold. (±)-β-Citronellol, a substrate for the acyclic terpene utilization pathway, was able to induce only promoter P2, by 2.4-fold (data not shown). The monocyclic R-(+)-limonene induced promoter P2 by approximately 4-fold and P6 by 3-fold, while the cyclic alcohol (−)-carveol induced only P2, by 2.4-fold (data not shown). The addition of (−)-α-terpineol did not result in substantial fluorescence levels of the reporter (below 1.5-fold) for any of the promoter regions tested. The bicyclic (−)-β-pinene mainly induced the activity of promoter P2, by 3-fold, as well as promoters P1 and P3 by approximately 2-fold.

DISCUSSION

This report describes the first functional characterization of a 28-kb GI associated with β-myrcene metabolism in *Pseudomonas* sp. M1. By monitoring the β-myrcene-induced expression of promoter reporter systems in different GI genotypes, the overall genetic organization of the 28-kb island was validated and the promoter activity was correlated with the biotransformation of β-myrcene, according to the predicted path-

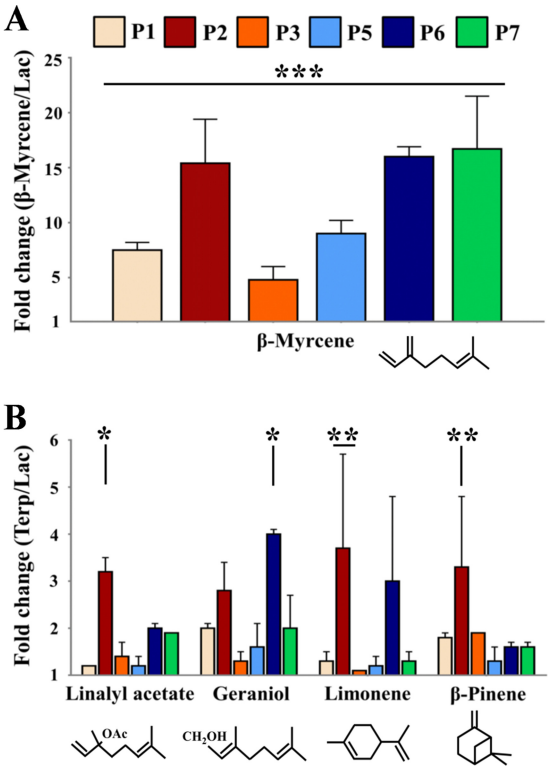

FIG 6 Activity of the promoter regions P1, P2, P3, P5, P6, and P7 in the presence of different monoterpenes. Cultures of M1 cells harboring the pSEVA637 constructs were supplemented with β-myrcene (A) and equimolar volumes of other monoterpenes (B), commonly used in industrial processes. Only those monoterpenes that showed significant activation of the promoter regions are depicted: linalyl acetate and geraniol (aliphatic), *R*-(+)-limonene (monocyclic) and (−)-β-pinene (bicyclic). GFP expression was measured after 5 h of incubation with 9.6 μmol of terpene substrate in solution. The promoter activity is shown as the fold induction ratio of the relative fluorescence units normalized by $OD_{600\ nm}$, between cells challenged with the monoterpene and control cells grown only with 48 mM lactate. Statistical significance was calculated by a two-way ANOVA test, using the fold change of lactate control (FC = 1) as a reference: *, $P < 0.05$; **, $P < 0.01$; ***, $P < 0.001$.

way (11, 13). In particular, the comparison performed between M1 wt and derived strains, based on promoter reporter activity and GC-MS identification of β-myrcene derivatives from biotransformation experiments, provided evidence for the involvement of genes organized within TU5 and TU6 in the initial oxidation steps of β-myrcene and their biotechnological relevance as targets for engineering approaches and development of β-myrcene catalysts. Moreover, the molecular and physiological approaches described in this work allowed the identification of two key gene products, essential to activate the β-myrcene core code in the 28-kb GI and to confer the ability to use this monoterpene as the sole carbon source in *Pseudomonas* sp. M1 cells: the novel putative β-myrcene hydroxylase (PM1_0216370), involved in the initial oxidation of the β-myrcene backbone (based mainly on experiments with strain M1-C38), and the one-component switch-like regulator (PM1_0216375), capable of readily sensing a β-myrcene-derived stimulus and of activating the 28-kb GI (based mainly on experiments with strain M1-C19). Considering the homology of the PM1_0216375 protein sequence with regulators from the MalT subfamily, this protein may alternate between a stable inactive monomeric conformation (which might be constitutively expressed at a low concentration) and an oligomeric active conformation when the inducer molecule is recognized. The induction of the active conformation could be performed by β-myrcene, or a β-myrcene-dependent stimulus, derived from the alterations occurring in the membrane (e.g., a physical stimulus derived from membrane stress or from the hydrophobic environment in the interface between the aqueous medium and β-myrcene droplets or an interaction with a signaling/sensor protein

located in the membrane). The active PM1_0216375 might activate the transcription of the membrane-bound β-myrcene hydroxylation system encoded by the TU5, comprised of the *PM1_0216370* and *PM1_0216365* gene products, for instance, by recruiting the RNA polymerase or altering the promoter region topology which leads to transcription initiation.

Additionally, the profiles of promoter reporter expression suggested the sequential activation of transcriptional units TU5 ≫ TU6 ≫ TU3 during β-myrcene catabolism, in which the initial hydroxylation of β-myrcene into myrcen-8-ol seemed to be an important trigger for the initial activation of the 28-kb GI. In particular, reporter analysis (Fig. 2) showed a dependence of the successful activation of TU6 (the dehydrogenase-encoding cluster *myrABC*) on the expression of TU5 gene products, whereas the induction of TU3, which was not active in M1-C19, M1-C38, or M1-N22, is in fact dependent on the successful recognition of β-myrcene stimulus and activation of TU5 and TU6 to carry the initial oxidations. This interplay between transcriptional units hints at a regulatory coordination, in which modulation by β-myrcene derivatives might be involved. Nevertheless, a putative activation mechanism mediated by metabolic intermediates does not fully explain the molecular outcomes registered. Both TU5 and TU6 (and other transcriptional units) might require additional regulatory elements to confer full metabolic potential to the 28-kb GI, as downregulation of the reporter GFP was observed in both strain M1-N22 and strain M1-C38 for promoters P5 and P6 (Fig. 2). Furthermore, a polar effect resulting from transposon insertion, altering transcription of downstream genes encoding the polycistronic mRNA molecule, could also affect the transposon-derived phenotypes. However, and particularly in the mutation of PM1_0216375 and PM1_0216370, the respective transcriptional units are not predicted to code for more than one key protein (the regulator or the β-myrcene hydroxylase), and thus, the transposon insertion was unlikely to cause downstream transcription inhibition, which is supported by the differences observed in the profile of promoter activity between strains M1-C19 and M1-C38 and mutant complementation.

Additionally, further molecular characterization will also focus on describing the role of the PM1_0216360 and PM1_0216405 regulators. As described for MalT in *E. coli* (25) and other regulators of the aromatic hydrocarbon catabolic pathways (e.g., XylS and XylR from *P. putida* TOL plasmid [26]), the regulatory protein PM1_0216375 might be synthesized constitutively in a residual concentration, becoming active only in the presence of the inducer. A similar mechanism could also occur in the P4-controlled PM1_0216360 regulator, which shows a one-component sensor-like structure similar to that of PM1_0216375. Thus, the absence of a significant increase in fold change of the reporter level of promoters P4 and P8 could be explained by a posttranslational modulation of the regulator activity, without a significant increase in the expression of the respective transcriptional unit upon β-myrcene induction.

Although the 28-kb GI from strain M1 might have evolved toward the specialized mineralization of β-myrcene, as shown by the reporter levels in Fig. 6A, this locus was also responsive to other monoterpenes, with concomitant biotransformation of the inducer compounds (Fig. 6B; see Table S4 in the supplemental material). In the M1 wt strain, promoter regions P2 and P6 (and to a lesser extent P1 and P3) were activated by acyclic (linalyl acetate) and cyclic [*R*-(+)-limonene and (−)-β-pinene] monoterpene backbones (or their derivatives): P2 was putatively involved in sensing a wide range of monoterpene-related molecules, while P6-controlled enzymes would be involved in the oxidation of different terpene alcohols. The putative gene products encoded by TU3, namely, the monooxygenase PM1_0216335 and epoxide hydrolase PM1_0216350, resemble the enzymatic machinery reported for the biotransformation of some cyclic monoterpenes (27–29) and could be involved in the oxidation or ring opening of cyclic backbones. Nevertheless, a comparison of monoterpenes was performed by using β-myrcene as a reference compound and was based on theoretical values regarding their chemical characterization (Table S1). The monoterpenes used showed different physicochemical properties (structure, volatility, solubility in aqueous medium, membrane partition) which influence substrate availability and, thus, the outcome of biological experi-

ments. Future work will focus on a detailed characterization of the response of strain M1 to β-myrcene and related monoterpenes, with respect to (i) the expression kinetics of the 28-kb GI TUs complemented with substrate titration, (ii) the effect of carbon sources/energetic balance on the performance of monoterpene biotransformation in cometabolism experiments, (iii) putative catabolic repression systems and cell adaptation mechanisms, and (iv) details on the possible regulatory cross-talks between secondary/redundant enzymatic systems, which might explain the broad range of monoterpene substrates of the 28-kb catabolic island and the ability of several M1 mutants (e.g., M1-N22) to overcome the disruption of the predicted central catabolic pathway for β-myrcene.

The versatility of the M1 enzymatic repertoire and the ability of M1 cells to maintain membrane integrity when different catabolic steps are impaired, and harmful metabolites are accumulated (e.g., myrcen-8-ol) (20, 30, 31), emphasize the environment-driven adaptation of this potential biochassis toward particular carbon sources derived from plant material and/or with highly hydrophobic characteristics. The metabolic tuning of strain M1, and in particular of the 28-kb GI, may prompt the development of optimized biochassis and bioblocks for tailored biotransformation of natural and nonnatural compounds, targeting industrial wastes and by-products as carbon feedstock for sustainable biotechnological processes. Furthermore, the functional elements characterized in this work might present potential targets for engineering strategies and incorporation as functional parts in plant volatile-responsive circuits.

MATERIALS AND METHODS

Bacterial strains, culture conditions, vectors, and primers used. Bacterial strains, plasmids, and primers used in this work are listed in Table 4 and Table 5, respectively. For molecular biology procedures, *Escherichia coli* and *Pseudomonas* sp. M1 strains were routinely maintained in Luria-Bertani (LB) medium, supplemented with antibiotics as follows: gentamicin at 30 μg ml^{-1}, or kanamycin at 50 μg ml^{-1}. β-Myrcene, (±)-β-citronellol, linalyl acetate (acetate ester of linalool), and (−)-α-terpineol were purchase from Merck. *R*-(+)-Limonene, (−)-β-pinene, (−)-carveol, and geraniol were purchased from Alfa Aesar. Analytical standards of fatty acid methyl esters for analysis of the membrane lipid content ($C_{16:0}$, $C_{16:1\ trans}$, $C_{16:1\ cis}$, $C_{18:0}$, $C_{18:1\ trans}$, $C_{18:1\ cis}$) were purchased from Sigma-Aldrich.

Construction of promoter probes to evaluate expression of different transcriptional units from the 28-kb β-myrcene genomic core. The molecular characterization of the transcriptional units from the 28-kb GI was performed by using a promoter probe reporter system. The promoter probes were constructed by coupling the eight promoter regions predicted *in silico* in the 28-kb GI of strain M1 by Soares-Castro and Santos (12), with the GFP reporter gene as transcriptional fusions. The promoter regions were amplified by PCR with primer sequences listed in Table 5, yielding DNA fragments flanked by BamHI and HindIII restriction sites. PCR amplification was performed according to the following protocol: initial denaturation step at 96°C for 3 min, 30 cycles of denaturation at 96°C for 30 s, annealing at 50°C for 30 s, and extension at 72°C for 45 s, followed by a final extension step at 72°C for 5 min. The amplification products were purified from agarose gel and cloned into the broad-host-range vector pSEVA637 (32).

Whole-genome mutagenesis targeting inactivation of the *PM1_0216320-PM1_0216325* sensory cluster (TU2). The mutagenesis strategy to identify putative activators of the *PM1_0216320-PM1_0216325* sensory cluster, comprising the predicted transcriptional unit 2 (TU2) of the 28-kb GI, was performed with the pBAM1 vector (33) harboring the P2::GFP reporter fusion.

The reporter transposon was constructed by cloning promoter P2 fused to GFP from pSEVA637-P2, flanked by BamHI/EcoRI (Table 5), into pBAM1, which resulted in the vector pBAM1-P2::GFP. pBAM1-P2::GFP was mobilized by standard biparental mating to strain M1, and colonies were screened for the loss of P2::GFP fluorescence by microscopy. From this mutagenesis approach, two mutant strains were isolated, M1-C19 and M1-C38.

Transposon insertion sites were amplified by arbitrary PCR, adapted from the report by Das et al. (34). Initially, the insertion site was amplified from the ME-I transposon end with primers ARB6/ME-I-extR and from the ME-O transposon end with primers ARB6/gfp-extF. The second PCR was performed with primers ARB2/ME-I-intR targeting the ME-I end and primers ARB2/gfp-intF targeting the ME-O end. The ARB6-related PCR was performed by using an initial denaturation step at 96°C for 3 min, 6 cycles of denaturation at 96°C for 30 s, annealing at 30°C for 30 s, and extension at 72°C for 90 s, followed by 30 cycles of denaturation at 96°C for 30 s, annealing at 45°C for 30 s, and extension at 72°C for 90 s, with a final extension step at 72°C for 5 min. The ARB2-related PCR was performed by using an initial denaturation step at 96°C for 3 min, 30 cycles of denaturation at 96°C for 30 s, annealing at 52°C for 30 s, and extension at 72°C for 90 s, with a final extension step at 72°C for 5 min. PCR products were purified and sequenced by use of an ABI 3730xl sequencer (Beckman Coulter Genomics).

Monitoring the activity of promoter reporters from the 28-kb GI in M1 strains. The pSEVA637 promoter probe constructs were mobilized into M1 strains (M1 wt, M1-N22, M1-C19, and M1-C38) by standard biparental mating on membranes, using *E. coli* S17.1λpir as the donor. Myrcene-dependent activity

TABLE 4 Bacterial strains and plasmids used in this work

Strain or plasmid	Description	Reference or source
Strains		
Escherichia coli S17.1λpir	*recA thi pro hsdR* M^+ RP4-2Tc::Mu-Km::Tn7 Tp^r Sm^r *λpir*; recipient strain for conjugation experiments	57
Pseudomonas sp. M1	Wild type; phenol, toluene, myrcene, cresol, citronellol, and citral positive	11
Pseudomonas sp. M1-N22	Derived from strain M1; mini-Tn*5*-Km cassette inserted in *myrB* (*PM1_0216390)*	11
Pseudomonas sp. M1-C19	Derived from strain M1; pBAM1-P2::GFP cassette inserted in *PM1_021675*	This work
Pseudomonas sp. M1-C38	Derived from strain M1; pBAM1-P2::GFP cassette inserted in *PM1_021670*	This work
Plasmids		
pSEVA637	GFP promoter probe vector for transcriptional fusions; pBBR1, Gm^r, 3.7 kbp	32
pSEVA637-P1	pSEVA637 derivative containing the promoter region P1 from the M1 28-kb GI; Gm^r, 4.0 kbp	This work
pSEVA637-P2	pSEVA637 derivative containing the promoter region P2 from the M1 28-kb GI; Gm^r, 4.2 kbp	This work
pSEVA637-P3	pSEVA637 derivative containing the promoter region P3 from the M1 28-kb GI; Gm^r, 4.2 kbp	This work
pSEVA637-P4	pSEVA637 derivative containing the promoter region P4 from the M1 28-kb GI; Gm^r, 4.0 kbp	This work
pSEVA637-P5	pSEVA637 derivative containing the promoter region P5 from the M1 28-kb GI; Gm^r, 3.9 kbp	This work
pSEVA637-P6	pSEVA637 derivative containing the promoter region P6 from the M1 28-kb GI; Gm^r, 4.0 kbp	This work
pSEVA637-P7	pSEVA637 derivative containing the promoter region P7 from the M1 28-kb GI; Gm^r, 4.0 kbp	This work
pSEVA637-P8	pSEVA637 derivative containing the promoter region P8 from the M1 28-kb GI; Gm^r, 4.1 kbp	This work
pBAM1	Tn*5*-derived vector for random mutagenesis; R6K, Km^r Amp^r, 4.4 kbp	33
pBAM1-P2::GFP	pBAM1 derivative containing the promoter region P2::GFP; R6K, Km^r Amp^r, 5.7 kbp	This work
pSEVA638	pSEVA238 derivative with Gm^r cassette; *xylS*-P*m*-based expression vector, pBBR1, 4.9 kbp	This work
pSEVA638-PM1_0216375	pSEVA638 derivative containing the promoterless *PM1_0216375* sequence; Gm^r, 5.2 kbp	This work
pSEVA638-TU5	pSEVA638 derivative containing the promoterless TU5 (*PM1_0216365-PM1_0216370*) sequence; Gm^r, 5.0 kbp	This work

levels of the assayed promoter regions were (i) monitored by fluorometric detection in a Qubit 3.0 fluorometer and expressed as the fold induction of GFP fluorescence normalized by the culture optical density measured at 600 nm ($OD_{600\ nm}$) between myrcene-induced and noninduced cells and/or (ii) confirmed by microscopy in a Leica DM5000B-CTR5000 fluorescence microscope (total magnification, ×400).

To validate the predicted promoter regions, overnight cultures of the M1 wt strain were refreshed in MM (35) supplemented with 48 mM lactate or 100 μl of β-myrcene (130 mg $liter^{-1}$, 47.8 μmol in solution) and cultures were diluted again at mid-exponential phase. As with the RNA-seq experiment described by Soares-Castro and Santos (12), when cultures reached an $OD_{600\ nm}$ of around 0.3 to 0.4, cells were collected to monitor the GFP reporter expression by microscopy in both carbon sources.

To monitor the reporter expression in the M1 mutant strains (M1-N22, M1-C19, M1-C38), cells were grown as described above in MM supplemented with 48 mM lactate. The promoter regions were induced by challenging M1 wt and mutant strains, harboring the GFP-based promoter reporters, with a saturating amount of 20 μl of β-myrcene (26 mg $liter^{-1}$, 9.6 μmol in solution) and measured 5 h after medium supplementation with the inducer. The β-myrcene-dependent activity levels were expressed as fold induction as described above and plotted in a heatmap by using the function heatmap.2 from R statistical software with the gplots package (36).

Phenotype complementation of M1-C38 and M1-C19 strains. To complement the transposon interruption of PM1_0216375 and PM1_0216370 in M1-C19 and M1-C38 strains, respectively, the promoterless *PM1_0216375* and TU5 (*PM1_0216365-PM1_0216370*) segments were amplified by PCR (Table 5). The *PM1_0216375* and TU5 products were digested with BamHI/SalI and EcoRI/SalI, respectively, and cloned into pSEVA638, which harbors the expression system *xylS*-P*m* (32). The resulting vectors (pSEVA638-PM1_0216375 and pSEVA638-TU5) were mobilized into M1-C19 and M1-C38 strains, respectively, by standard biparental mating as described above. Phenotype complementation was evaluated by assessing the ability of M1-C19 (pSEVA638-PM1_0216375) and M1-C38 (pSEVA638-TU5) strains to grow in MM supplemented with β-myrcene as the sole carbon source, in the presence of the inducer 3-methylbenzoate.

Evaluation of the monoterpene substrate spectrum of the 28-kb GI. In order to identify the potential substrates of the 28-kb β-myrcene core code, M1 wt cells harboring the transcriptional fusion of promoters expressing the GFP reporter were cultured in MM supplemented with 48 mM lactate, as

TABLE 5 Primers used in this work

Primer	Sequence (5′–3′)	Vector
Transcriptional fusion primers		
P1-FWD-gfp-BamHI	AATAGGATCCTCATGCTCGCCAGTGGACG	pSEVA637-P1
P1-REV-gfp-HindIII	AGAGAAGCTTTTACACAGTTCCCCAGCATGC	pSEVA637-P1
P2-FWD-gfp-HindIII	AGCAAAGCTTTTCACCCCCGAGCATGGG	pSEVA637-P2
P2-REV-gfp-BamHI	AATTGGATCCGTCTTGCCTCCTCATCCC	pSEVA637-P2
P3-FWD-gfp-BamHI	AACTGGATCCTTCACCCCCGAGCATGGG	pSEVA637-P3
P3-REV-gfp-HindIII	ACGAAAGCTTGTCTTGCCTCCTCATCCC	pSEVA637-P3
P4-FWD-gfp-HindIII	AACTAAGCTTCACCAGTTGCGGGGGAGATTG	pSEVA637-P4
P4-REV-gfp-BamHI	ATTAGGATCCTCTACGACGAAGCATTGGG	pSEVA637-P4
P5-FWD-gfp-HindIII	AACTAAGCTTAGTGCCTCCACGGCGTTTGC	pSEVA637-P5
P5-REV-gfp-BamHI	ATTAGGATCCACTCCCACCCGCCCATTTCC	pSEVA637-P5
P6-FWD-gfp-HindIII	AACTAAGCTTGCGCCGAATGTCGGCGCTTTGAG	pSEVA637-P6
P6-REV-gfp-BamHI	ATTAGGATCCAAGAAAGGGAAGGATCGCGC	pSEVA637-P6
P7-FWD-gfp-BamHI	AACAGGATCCGCGCCGAATGTCGGCGCTTTGAG	pSEVA637-P7
P7-REV-gfp-HindIII	ACTGAAGCTTAAGAAAGGGAAGGATCGCGC	pSEVA637-P7
P8-FWD-gfp-BamHI	AACAGGATCCTGTCTGGCCCGAGTCTGGC	pSEVA637-P8
P8-REV-gfp-HindIII	ACTGAAGCTTTACTCCACCCTCTCCATTGGC	pSEVA637-P8
Whole-genome mutagenesis primers		
P2::GFP -FWD-BamHI	ATTTGGATCCGTCTTGCCTCCTCATCCC	pBAM-P2:GFP
P2::GFP -REV-EcoRI	GATGGAATTCCTGGATTCTCACCAATAAAAAACGC	pBAM-P2:GFP
ARB6	GGCACGCGTCGACTAGTACNNNNNNNNNNACGCC	Check insertion site of the transposon
ME-I-extR	CTCGTTTCACGCTGAATATGGCTC	
gfp-extF	CGATGGCCCTGTCCTTTTACC	
ARB2	GGCACGCGTCGACTAGTAC	
ME-I-intR	CAGTTTTATTGTTCATGATGATATA	
gfp-intF	TTCAGAACGCTCGGTTGCCG	
Complementation primers		
TU5-FWD	TATAGAATTCATGAGTACCGTCACCCCAAAGG	pSEVA638-TU5
TU5-REV	AAAAGTCGACTCAGATCTCGTCGAAATCGAC	pSEVA638-TU5
PM1_0216375-FWD	ATATGGATCCATGAAGACCTGCTTGCAGCC	pSEVA638-PM1_0216375
PM1_0216375-REV	TAAAGTCGACTTACTCGCCGTGGTTCAGTAG	pSEVA638-PM1_0216375

described above. Culture medium was supplemented with monoterpenes that were structurally related to β-myrcene, and the promoter activity was measured at 5 h after stimulus. The molarity of the different monoterpenes was calculated as described in the supplemental material (Table S1) (37, 38), taking into account the different physicochemical properties (e.g., solubility in aqueous medium and vapor pressure) and their influence in the bioavailability of each monoterpene in the assay. Saturating amounts of β-myrcene were used as a reference (20 μl, corresponding to 9.6 μmol in solution), and the promoter activity levels were expressed as fold induction of normalized GFP fluorescence, as described previously. The statistical significance of the differences in fold change was analyzed by a two-way analysis of variance (ANOVA) test, with comparisons to the fold change of the lactate control.

Qualitative GC-MS analysis of terpene derivatives from cultures of *Pseudomonas* sp. M1 and derived strains, supplemented with plant-derived volatiles. *Pseudomonas* sp. M1 and derived strains were cultured as described for the evaluation of the reporter activity in 50 ml of MM using lactate as the carbon source and supplemented with 5 μl of the following monoterpene compounds for identification of the respective oxidative products. Cultures of the wild-type strain of *Pseudomonas* sp. M1 were supplemented with β-myrcene, (±)-β-citronellol, linalyl acetate, *R*-(+)-limonene, and (−)-β-pinene, whereas biotransformation experiments with the M1-derived strains were performed only with β-myrcene.

To extract terpene derivatives from biotransformation experiments, cultures were prepared for each time point analyzed, in which 50 ml of the supernatant (the whole culture) was collected, mixed with 10 ml ethyl acetate, and vigorously shaken for 5 min. The ethyl acetate extracts were dried with a nitrogen gas stream, dissolved in 1 ml of hexane, and concentrated with a nitrogen gas stream to a final volume of around 500 μl, for subsequent GC-MS analysis. Control metabolite profiles were prepared by using (i) pure terpene standards extracted in hexane; (ii) culture supernatants from cells grown in lactate as the sole carbon source without supplementation with terpenes, at different time points, to rule out the metabolite profile of different growth stages; and (iii) an abiotic control of MM with lactate and terpene supplementation.

The gas chromatography analysis of the supernatants from biotransformation experiments was performed on a model 7890A GC-5975C inert XL MSD system, coupled to a model 7693 automatic liquid sampler and equipped with a J&W HP-INNOWax polar capillary column (polyethylene glycol; 30 m by 0.25-mm inside diameter by 0.25-μm film thickness) (all from Agilent Technologies). Helium was used as the carrier gas at a flow rate of 1.6 ml min^{-1}, and 1 μl of sample was injected in the splitless mode. The column temperature was initially kept at 60°C for 1 min and then was gradually increased to 250°C at a rate of 10°C min^{-1}, with a final hold time of 2 min (adapted from references 39 and 40). The mass spectra

were acquired with an electron impact ionization voltage of 70 eV, scanned in the *m/z* range of 40 to 500 amu. Cultures of β-myrcene biotransformed with M1 strains were assayed in quadruplicate (wt strain) and triplicate (mutant strains) up to 3.5 h after the addition of the monoterpene. Biotransformations of the other monoterpenes by the wt strain were assayed at two time points (4 h and 20 h). The baseline of the obtained chromatograms was defined with the statistics-sensitive nonlinear iterative peak-clipping algorithm (41, 42), which showed to be the best fit for the shape of different peak-free regions throughout the chromatogram.

Metabolite identification. The total ion chromatograms were deconvoluted with the AMDIS tool version 2.71 (43) to generate the ion spectra for every integer *m/z* component in the data acquisition range of atomic mass units. The deconvoluted *m/z* spectra whose intensity values increase, maximize, and decrease together are derived from the same chemical species and thus comprise its ion profile used for compound identification. The filtered ion profile of each chemical species (here defined as the query peak) was obtained by subtracting the intensity of the *m/z* components from the matrix (region of the GC-MS spectrum without peaks) and/or from adjacent peaks on either side of the query peak. The ion profile of overlapped peaks, corresponding to coeluted compounds, was manually filtered by subtracting the intensity of the *m/z* components of the contaminant peak from the ion profile of the query peak.

The identification of terpene derivatives was done based on (i) the National Institute of Standards and Technology (NIST) MS Search tool version 2.0 libraries (mainlib comprising 163,198 spectra and Wiley Registry of Mass Spectral Data comprising 228,996 spectra), (ii) by comparing calculated retention indices (RI) with those reported in the literature and/or from the NIST Mass Spectrometry Data Center (44), and (iii) validation with commercial compounds when available. Retention indices of each query compound were determined by sampling a mixture of *n*-alkanes (C_{10} to C_{28}) under the same GC-MS conditions (45).

Membrane fatty acid profile and viability of cells challenged with β-myrcene. Cultures of *Pseudomonas* sp. M1 strains, prepared as described for the evaluation of the expression of promoter probes, were grown in MM supplemented with lactate and exposed to 20 μl of β-myrcene. Cells were collected after 0.5 h, 1.5 h, and 3 h of monoterpene addition for lipid extraction. Cell viability was evaluated in parallel after 3 h of the 20-μl β-myrcene pulse, by diluting and plating cells in LB agar plates for CFU counting. Cultures without β-myrcene supplementation were used as a control. The specific growth rate (μ) for each strain growing in lactate (μ_{lac}) or lactate with β-myrcene pulse (μ_{myr}), during the assayed time points, was calculated and expressed as a ratio of μ_{myr} to μ_{lac}, to correlate changes in the cell envelope with cell viability and growth rate during β-myrcene biotransformation.

For the analysis of the fatty acid profile, the collected cell pellets were washed with 10 mM potassium nitrate and the FAMEs were prepared as described by Morrison and Smith (46) and Piotrowska et al. (47). Lipids were extracted from cells with methanol and chloroform. The lipid-containing chloroform phase was dried in a nitrogen gas stream, the transesterification of fatty acids was performed with boron trifluoride-methanol for 15 min at 96°C, and FAMEs were extracted in hexane. The FAMEs were analyzed in a model 6890N GC system with a flame ionization detector and equipped with a CP-SIL 88 50-m capillary column (Agilent Technologies). Authentic reference compounds were coinjected with samples. FAMEs were separated at an initial temperature of 40°C for 2 min, followed by an increase of 8°C min^{-1} up to 220°C, with a final hold of 10 min. The peak areas were used to determine the relative amounts of each fatty acid. The degree of saturation of membrane fatty acids was defined as the ratio of saturated $C_{16:0}$ and $C_{18:0}$ to unsaturated $C_{16:1}$ and $C_{18:1}$ fatty acids. The *trans*/*cis* ratio of unsaturated fatty acids was defined as the ratio between the amounts of the two *trans* unsaturated fatty acids (16:1 *trans*, 18:1 *trans*) and the two *cis* unsaturated fatty acids (16:1 *cis*, 18:1 *cis*) of *Pseudomonas* strains (47).

In silico analysis of protein sequences from PM1_0216375 and PM1_0216370. The protein sequence of PM1_0216375 was compared with the sequences of eight major families of transcriptional regulators involved in the catabolism of acyclic and cyclic/aromatic hydrocarbons, as described by Tropel and van der Meer (48). Sequences were retrieved from UniProt and aligned by the MAFFT L-INS-i method (49), and a similarity tree was generated with PhyML version 2.4 (50), with 100 bootstrap sets, the best-fit model of amino acid substitution for maximal likelihood predicted by Prottest version 3 (51), kappa estimated, gamma distribution parameter estimated, BIONJ starting tree, with optimization of topology, branch lengths, and rate parameter. The functional domains of PM1_0216375 sequence were predicted by InterPro (52) and used for a detailed analysis of the identity of amino acid residues with the respective homologous regions in other characterized MalT-like regulators: MalT from *Escherichia coli* (UniProt accession no. P06993), AcoK from *Klebsiella pneumoniae* (UniProt accession no. Q48411), AlkS from *Pseudomonas putida* GPo1, formerly *Pseudomonas oleovorans* (UniProt accession no. P17051), and AlkS from *Pseudomonas putida* P1 (UniProt accession no. Q9L4M7).

The protein sequence of PM1_0216370 was compared with the sequence of membrane nonheme di-iron proteins by homology search with blastp (53) and prediction of functional domains with InterPro (52). For a detailed analysis, transmembrane domains in the PM1_0216370 protein sequence were predicted by a Kyte-Doolittle hydropathy plot, obtained from the Protscale tool of the Expasy server (54, 55), using a window size of 19 amino acids. For the homology-based clustering analysis, the protein sequences from PM1_0216370 and reported membrane nonheme hydroxylases, monooxygenases, and fatty acid desaturases were retrieved from UniProt and aligned by the MAFFT E-INS-i method. The region comprising the conserved histidine-rich motifs $HX_{3-4}H$, $HX_{2-3}HH$, and HXXHH, described by Shanklin et al. (56), were used to generate the similarity tree as described above. The accession numbers of the protein sequences used are as follows: Q8YQ27, *Nostoc* sp. strain PCC7120; AAP99312, *Prochlorococcus marinus* CCMP1375; A3WE62, *Erythrobacter* sp. strain NAP1; O85832, *Novosphingobium aromaticivorans*; P94792, *Flavobacterium* sp. ATCC 21588; Q44262, *Paracoccus* sp. strain PC1; Q01332, *Escherichia vulneris*; P21688, *Pantoea ananas*; Q88HV7, *P. putida* KT2440; A6N7G2, *Psychrobacter urativorans*; Q12SQ0, *Shewanella*

denitrificans OS217; P12691, *P. oleovorans* (currently *P. putida* GPo1); O31250, *Acinetobacter baylyi* ADP1; Q9AEN3, *Burkholderia cepacia* RR10; E5G6V9, *Rhodococcus aetherivorans* BCP1; P21395, *P. putida* KT2440; and O33456, *P. putida* F1.

SUPPLEMENTAL MATERIAL

Supplemental material for this article may be found at https://doi.org/10.1128/AEM.03112-16.

SUPPLEMENTAL FILE 1, PDF file, 1.5 MB.

ACKNOWLEDGMENTS

Vectors from the Standard European Vector Architecture (SEVA) library and pBAM1 used in this work were kindly provided by Victor de Lorenzo (CNB-CSIC, Madrid, Spain).

This work was supported by the strategic program UID/BIA/04050/2013 (POCI-01-0145-FEDER-007569) funded by national funds through the FCT I.P. and by the ERDF through the COMPETE2020-Programa Operacional Competitividade e Internacionalização (POCI) and through a Ph.D. grant (grant SFRH/BD/76894/2011) to P.S.-C.

REFERENCES

1. Hocquemiller R, Cortes D, Arango GJ, Myint SH, Cavé A, Angelo A, Muñoz V, Fournet A. 1991. Isolation and synthesis of espintanol, a new antiparasitic monoterpene. J Nat Prod 54:445–452. (In French.) https://doi.org/10.1021/np50074a015.
2. van der Werf M, de Bont JM, Leak D. 1997. Opportunities in microbial biotransformation of monoterpenes, p 147–177. *In* Berger RG, Babel W, Blanch HW, Cooney CL, Enfors SO, Eriksson KEL, Fiechter A, Klibanov AM, Mattiasson B, Primrose SB, Rehm HJ, Rogers PL, Sahm H, Schügerl K, Tsao GT, Venkat K, Villadsen J, von Stockar U, Wandrey C (ed), Biotechnology of aroma compounds. Springer, Berlin, Germany.
3. Crowell PL. 1999. Prevention and therapy of cancer by dietary monoterpenes. J Nutr 129:775.
4. Rasooli I, Mirmostafa SA. 2003. Bacterial susceptibility to and chemical composition of essential oils from *Thymus kotschyanus* and *Thymus persicus*. J Agric Food Chem 51:2200–2205. https://doi.org/10.1021/jf0261755.
5. Heipieper HJ, Neumann G, Cornelissen S, Meinhardt F. 2007. Solvent-tolerant bacteria for biotransformations in two-phase fermentation systems. Appl Microbiol Biotechnol 74:961–973. https://doi.org/10.1007/s00253-006-0833-4.
6. Krings U, Berger GR. 1998. Biotechnological production of flavours and fragrances. Appl Microbiol Biotechnol 49:1–8. https://doi.org/10.1007/s002530051129.
7. Schwab W, Fuchs C, Huang F-C. 2013. Transformation of terpenes into fine chemicals. Eur J Lipid Sci Technol 115:3–8. https://doi.org/10.1002/ejlt.201200157.
8. Held M, Schmid A, van Beilen JB, Witholt B. 2000. Biocatalysis. Biological systems for the production of chemicals. Pure Appl Chem 72:1337–1343.
9. Boyle PM, Silver PA. 2012. Parts plus pipes: synthetic biology approaches to metabolic engineering. Metab Eng 14:223–232. https://doi.org/10.1016/j.ymben.2011.10.003.
10. Smanski MJ, Zhou H, Claesen J, Shen B, Fischbach MA, Voigt CA. 2016. Synthetic biology to access and expand nature's chemical diversity. Nat Rev Microbiol 14:135–149. https://doi.org/10.1038/nrmicro.2015.24.
11. Iurescia S, Marconi AM, Tofani D, Gambacorta A, Paternò A, Devirgiliis C, van der Werf MJ, Zennaro E. 1999. Identification and sequencing of β-myrcene catabolism genes from *Pseudomonas* sp. strain M1. Appl Environ Microbiol 65:2871–2876.
12. Soares-Castro P, Santos PM. 2014. Deciphering the genome repertoire of *Pseudomonas* sp. M1 toward β-myrcene biotransformation. Genome Biol Evol 7:1–17. https://doi.org/10.1093/gbe/evu254.
13. Santos PM, Sá-Correia I. 2009. Adaptation to β-myrcene catabolism in *Pseudomonas* sp. M1: an expression proteomics analysis. Proteomics 9:5101–5111. https://doi.org/10.1002/pmic.200900325.
14. Santos PM, Roma V, Benndorf D, von Bergen M, Harms H, Sá-Correia I. 2007. Mechanistic insights into the global response to phenol in the phenol-biodegrading strain *Pseudomonas* sp. M1 revealed by quantitative proteomics. OMICS 11:233–251.
15. Zubyk WJ, Conner AZ. 1960. Analysis of terpene hydrocarbons and related compounds by gas chromatography. Anal Chem 32:912–917. https://doi.org/10.1021/ac60164a004.
16. IOFI Working Group on Methods of Analysis. 2011. Guidelines for the quantitative gas chromatography of volatile flavouring substances, from the Working Group on Methods of Analysis of the International Organization of the Flavor Industry (IOFI). Flavour Fragr J 26:297–299.
17. Deininger S-O, Cornett DS, Paape R, Becker M, Pineau C, Rauser S, Walch A, Wolski E. 2011. Normalization in MALDI-TOF imaging datasets of proteins: practical considerations. Anal Bioanal Chem 401:167–181. https://doi.org/10.1007/s00216-011-4929-z.
18. Narushima H, Omori T, Minoda Y. 1982. Microbial oxidation of beta-myrcene, p 525–531. *In* Vezina C, Singh K (ed), Advances in biotechnology. Pergamon Press, Oxford, United Kingdom.
19. Sikkema J, de Bont JA, Poolman B. 1994. Interactions of cyclic hydrocarbons with biological membranes. J Biol Chem 269:8022–8028.
20. Turina AV, Nolan MV, Zygadlo JA, Perillo MA. 2006. Natural terpenes: self-assembly and membrane partitioning. Biophys Chem 122:101–113. https://doi.org/10.1016/j.bpc.2006.02.007.
21. Danot O, Marquenet E, Vidal-Ingigliardi D, Richet E. 2009. Wheel of life, wheel of death: a mechanistic insight into signaling by STAND proteins. Structure 17:172–182. https://doi.org/10.1016/j.str.2009.01.001.
22. Chen J, Xie J. 2011. Role and regulation of bacterial LuxR-like regulators. J Cell Biochem 112:2694–2702. https://doi.org/10.1002/jcb.23219.
23. Hsu J-L, Peng H-L, Chang H-Y. 2008. The ATP-binding motif in AcoK is required for regulation of acetoin catabolism in *Klebsiella pneumoniae* CG43. Biochem Biophys Res Commun 376:121–127. https://doi.org/10.1016/j.bbrc.2008.08.103.
24. Shanklin J, Whittle E. 2003. Evidence linking the *Pseudomonas oleovorans* alkane ω-hydroxylase, an integral membrane diiron enzyme, and the fatty acid desaturase family. FEBS Lett 545:188–192. https://doi.org/10.1016/S0014-5793(03)00529-5.
25. Marquenet E, Richet E. 2010. Conserved motifs involved in ATP hydrolysis by MalT, a signal transduction ATPase with numerous domains from *Escherichia coli*. J Bacteriol 192:5181–5191. https://doi.org/10.1128/JB.00522-10.
26. Domínguez-Cuevas P, González-Pastor J-E, Marqués S, Ramos J-L, de Lorenzo V. 2006. Transcriptional tradeoff between metabolic and stress-response programs in *Pseudomonas putida* KT2440 cells exposed to toluene. J Biol Chem 281:11981–11991. https://doi.org/10.1074/jbc.M509848200.
27. Yoo SK, Day DF. 2002. Bacterial metabolism of α- and β-pinene and related monoterpenes by *Pseudomonas sp*. strain PIN. Process Biochem 37:739–745. https://doi.org/10.1016/S0032-9592(01)00262-X.
28. van der Werf MJ, Overkamp KM, de Bont JAM. 1998. Limonene-1,2-epoxide hydrolase from *Rhodococcus erythropolis* DCL14 belongs to a novel class of epoxide hydrolases. J Bacteriol 180:5052–5057.
29. van der Werf MJ, Boot AM. 2000. Metabolism of carveol and dihydrocarveol in *Rhodococcus erythropolis* DCL14. Microbiology 146:1129–1141. https://doi.org/10.1099/00221287-146-5-1129.
30. Bard M, Albrecht MR, Gupta N, Guynn CJ, Stillwell W. 1988. Geraniol

interferes with membrane functions in strains of *Candida* and *Saccharomyces*. Lipids 23:534–538. https://doi.org/10.1007/BF02535593.
31. Griepernau B, Leis S, Schneider MF, Sikor M, Steppich D, Böckmann RA. 2007. 1-Alkanols and membranes: a story of attraction. Biochim Biophys Acta 1768:2899–2913. https://doi.org/10.1016/j.bbamem.2007.08.002.
32. Silva-Rocha R, Martínez-García E, Calles B, Chavarría M, Arce-Rodríguez A, de las Heras A, Páez-Espino AD, Durante-Rodríguez G, Kim J, Nikel PI, Platero R, de Lorenzo V. 2013. The Standard European Vector Architecture (SEVA): a coherent platform for the analysis and deployment of complex prokaryotic phenotypes. Nucleic Acids Res 41:D666–D675. https://doi.org/10.1093/nar/gks1119.
33. Martínez-García E, Calles B, Arévalo-Rodríguez M, de Lorenzo V. 2011. pBAM1: an all-synthetic genetic tool for analysis and construction of complex bacterial phenotypes. BMC Microbiol 11:38. https://doi.org/10.1186/1471-2180-11-38.
34. Das S, Noe JC, Paik S, Kitten T. 2005. An improved arbitrary primed PCR method for rapid characterization of transposon insertion sites. J Microbiol Methods 63:89–94. https://doi.org/10.1016/j.mimet.2005.02.011.
35. Hartmans S, Smits JP, van der Werf MJ, Volkering F, de Bont JAM. 1989. Metabolism of styrene oxide and 2-phenylethanol in the styrene-degrading *Xanthobacter* strain 124X. Appl Environ Microbiol 55:2850–2855.
36. Warnes GR, Bolker B, Bonebakker L, Gentleman R, Liaw WH, Lumley T, Maechler M, Magnusson A, Moeller S, Schwartz M, Venables B. 2016. gplots: various R programming tools for plotting data, version 3.0.1. http://cran.r-project.org/web/packages/gplots/index.html.
37. Cheng W-H, Chou M-S, Perng C-H, Chu F-S. 2004. Determining the equilibrium partitioning coefficients of volatile organic compounds at an air-water interface. Chemosphere 54:935–942. https://doi.org/10.1016/j.chemosphere.2003.08.038.
38. Sander R. 2015. Compilation of Henry's law constants (version 4.0) for water as solvent. Atmos Chem Phys 15:4399–4981. https://doi.org/10.5194/acp-15-4399-2015.
39. Holubová V, Hrdlička P, Kubáň V. 2001. Age and space distributions of monoterpenes in fresh needles of *Picea abies* (L) Karst. determined by gas chromatography-mass spectrometry. Phytochem Anal 12:243–249. https://doi.org/10.1002/pca.591.
40. Thompson ML, Marriott R, Dowle A, Grogan G. 2010. Biotransformation of β-myrcene to geraniol by a strain of *Rhodococcus erythropolis* isolated by selective enrichment from hop plants. Appl Microbiol Biotechnol 85:721–730. https://doi.org/10.1007/s00253-009-2182-6.
41. Ryan CG, Clayton E, Griffin WL, Sie SH, Cousens DR. 1988. SNIP, a statistics-sensitive background treatment for the quantitative analysis of PIXE spectra in geoscience applications. Nucl Instrum Methods Phys Res B 34:396–402. https://doi.org/10.1016/0168-583X(88)90063-8.
42. Morháč M. 2009. An algorithm for determination of peak regions and baseline elimination in spectroscopic data. Nucl Instrum Methods Phys Res A 600:478–487. https://doi.org/10.1016/j.nima.2008.11.132.
43. Stein SE. 1999. An integrated method for spectrum extraction and compound identification from gas chromatography/mass spectrometry data. J Am Soc Mass Spectrom 10:770–781. https://doi.org/10.1016/S1044-0305(99)00047-1.
44. Stein SE. Retention indices. *In* NIST Chemistry WebBook, NIST standard reference database number 69. National Institute of Standards and Technology, Gaithersburg MD.
45. van Den Dool H, Dec Kratz P. 1963. A generalization of the retention index system including linear temperature programmed gas-liquid partition chromatography. J Chromatogr A 11:463–471. https://doi.org/10.1016/S0021-9673(01)80947-X.
46. Morrison WR, Smith LM. 1964. Preparation of fatty acid methyl esters and dimethylacetals from lipids with boron fluoride-methanol. J Lipid Res 5:600–608.
47. Piotrowska A, Syguda A, Chrzanowski Ł, Heipieper HJ. 2016. Toxicity of synthetic herbicides containing 2,4-D and MCPA moieties towards *Pseudomonas putida* mt-2 and its response at the level of membrane fatty acid composition. Chemosphere 144:107–112. https://doi.org/10.1016/j.chemosphere.2015.08.067.
48. Tropel D, van der Meer JR. 2004. Bacterial transcriptional regulators for degradation pathways of aromatic compounds. Microbiol Mol Biol Rev 68:474–500. https://doi.org/10.1128/MMBR.68.3.474-500.2004.
49. Katoh K, Standley DM. 2013. MAFFT multiple sequence alignment software version 7: improvements in performance and usability. Mol Biol Evol 30:772–780. https://doi.org/10.1093/molbev/mst010.
50. Guindon S, Dufayard J-F, Lefort V, Anisimova M, Hordijk W, Gascuel O. 2010. New algorithms and methods to estimate maximum-likelihood phylogenies: assessing the performance of PhyML 3.0. Syst Biol 59:307–321. https://doi.org/10.1093/sysbio/syq010.
51. Abascal F, Zardoya R, Posada D. 2005. ProtTest: selection of best-fit models of protein evolution. Bioinformatics 21:2104–2105. https://doi.org/10.1093/bioinformatics/bti263.
52. Mitchell A, Chang H-Y, Daugherty L, Fraser M, Hunter S, Lopez R, McAnulla C, McMenamin C, Nuka G, Pesseat S, Sangrador-Vegas A, Scheremetjew M, Rato C, Yong S-Y, Bateman A, Punta M, Attwood TK, Sigrist CJA, Redaschi N, Rivoire C, Xenarios I, Kahn D, Guyot D, Bork P, Letunic I, Gough J, Oates M, Haft D, Huang H, Natale DA, Wu CH, Orengo C, Sillitoe I, Mi H, Thomas PD, Finn RD. 2015. The InterPro protein families database: the classification resource after 15 years. Nucleic Acids Res 43:D213–D221. https://doi.org/10.1093/nar/gku1243.
53. Altschul SF, Gish W, Miller W, Myers EW, Lipman DJ. 1990. Basic local alignment search tool. J Mol Biol 215:403–410. https://doi.org/10.1016/S0022-2836(05)80360-2.
54. Fauchere JL, Pliska V. 1983. Hydrophobic parameters π of aminoacid side-chains from the partitioning of N-acetyl aminoacid amide. Eur J Med Chem 18:369–375.
55. Gasteiger E, Hoogland C, Gattiker A, Duvaud S, Wilkins MR, Appel RD, Bairoch A. 2005. Protein identification and analysis tools on the ExPASy server, p 571–607. *In* Walker JM (ed), The proteomics protocols handbook. Humana Press, Totowa, NJ.
56. Shanklin J, Whittle E, Fox BG. 1994. Eight histidine residues are catalytically essential in a membrane-associated iron enzyme, stearoyl-CoA desaturase, and are conserved in alkane hydroxylase and xylene monooxygenase. Biochemistry 33:12787–12794. https://doi.org/10.1021/bi00209a009.
57. de Lorenzo V, Cases I, Herrero M, Timmis KN. 1993. Early and late responses of TOL promoters to pathway inducers: identification of post-exponential promoters in *Pseudomonas putida* with *lacZ-tet* bicistronic reporters. J Bacteriol 175:6902–6907. https://doi.org/10.1128/jb.175.21.6902-6907.1993.